RSC Advances

PAPER

View Article Online
View Journal | View Issue

Check for updates

Cite this: *RSC Adv.*, 2020, **10**, 12318

Surface states mediated charge transfer in redox behavior of hemin at GaAs(100) electrodes†

Mirela Enache,[a] Catalin Negrila[b] and Valentina Lazarescu*[a]

EIS and XPS investigations on the interaction of hemin with p- and n-doped GaAs(100) electrodes in PBS solution revealed significant differences concerning both the adsorbed species and the mechanism of the redox process caused by dopant nature. XPS data show that hemin is adsorbed on p-GaAs(100) by its carboxyl groups and adopts a vertical position favorable to a polymeric film formation whereas on n-GaAs(100), the adsorbed hemin is monomeric and has a rather planar configuration involving mainly the OH groups of the organic molecule. Hemin gives rise to a reversible redox process at the p-GaAs(100) electrode whereas at n-GaAs(100), there is only one reduction wave of a considerably lower current density appearing at a more negative potential. The effects of the applied potential on the phase angle measured at p-GaAs(100) point out major changes not only in the insulating properties of the adsorbed layer, as found at n-GaAs(100), but also in the electronic properties of the semiconductor triggered by the hemin redox process. Analysis of the experimental data points to a mechanism of charge transfer through surface states, the observed differences being related to the location of the surface states with respect to the formal potential of the hemin redox couple.

Received 17th February 2020
Accepted 20th March 2020

DOI: 10.1039/d0ra01508c

rsc.li/rsc-advances

Open Access Article. Published on 26 March 2020. Downloaded on 2/4/2026 3:08:19 AM.
This article is licensed under a Creative Commons Attribution-NonCommercial 3.0 Unported Licence.

1. Introduction

Hemin (iron protoporphyrin IX) is an important biological substance, being the active center of several families of heme proteins, such as C-type cytochromes, hemoglobin and myoglobin. Having a planar porphyrin ring containing four nitrogen atoms that may easily coordinate the iron ion capable of six-fold coordination, hemin is an attractive candidate for both basic and applied studies. The two additional coordination positions available above and below the porphyrine plane and the two carboxylic groups bring the possibility of different reaction sites playing a crucial role in determining its chemical binding and activity on solid surfaces. Chemical functionalization with hemin was thereby used to tune the substrates electronic properties for various applications. Hemin adsorbed on carbon substrates proved to be sensitive for the detection of hydrogen peroxide,[1,2] superoxide radicals[3] and oxygen,[4] and showed high electrocatalytic activity for reduction of nitrosamine[5] and hydroxylamine at low potentials in buffered neutral aqueous solutions.[6]

Functionalization of some III–V semiconductor compounds such as, GaAs, InAs and InP, with hemin is considered a promising route for new NO sensors design[7–9] due to the strong binding affinity of hemin to this small molecule. In this perspective, information concerning the charge transfer processes occurring at semiconductor/hemin contact can be exploited for using such hybrid organic–inorganic interfaces as sensors or detectors.[10]

Studying the redox behaviour of hemin on differently doped GaAs electrodes might be, therefore, relevant for understanding better the factors controlling this charge transfer process. Our previous investigations pointed out significant differences between the p- and n-doped GaAs electrodes in this respect. Cyclic voltammetry (CV) and impedance spectroscopy investigations (EIS) performed at p-GaAs(100) electrodes in phosphate buffer solutions with pH 7.45 revealed a pair of reversible peaks at −0.44 and −0.32 V *vs.* SCE resulting in stable adsorbed species[11] that turned out to be responsible for significant changes in the surface state population and the potential drop distribution between the semiconductor space charge region and the Helmholtz layer. The same combination of CV and EIS measurements on the redox behavior of hemin at n-GaAs(110) electrodes, but in a different solvent, dimethylsulfoxide, indicated, however, a pronounced irreversibility of the electroreduction process which was related to different chemical bonds of the reactant and the reaction product. The further examination of the hemin-covered GaAs electrodes by second harmonic generation, X-ray photoelectron spectroscopy and atomic force microscopy pointed to a possible change in the spin configuration of the iron ions preceding the charge transfer step originating in the mutual interactions between solvent, hemin and surface sites.[12] Since surface states and field

[a]*Institute of Physical Chemistry "Ilie Murgulescu", Spl. Independentei 202, P.O. Box 12-194, RO-060041, Bucharest, Romania. E-mail: vlazarescu@icf.ro*

[b]*National Institute of Material Physics, P.O. Box MG7, RO-77125 Bucharest, Romania*

† Electronic supplementary information (ESI) available: Energy bands diagram. See DOI: 10.1039/d0ra01508c

This journal is © The Royal Society of Chemistry 2020

Open Access Article. Published on 26 March 2020. Downloaded on 2/4/2026 3:08:19 AM.
This article is licensed under a Creative Commons Attribution-NonCommercial 3.0 Unported Licence.

effects were found to depend significantly at GaAs electrodes on both the surface orientation[13] and the charge carrier type,[14–17] the comparison between the redox behaviour of hemin on Si- and Zn-doped GaAs(100) in the same electrolyte should give a good hint about the role played by the charge carrier type in this charge transfer process. It is the aim of this paper to present the results of our electrochemical impedance spectroscopy (EIS) and X-ray photoelectron spectroscopy (XPS) investigations in this respect.

2. Experimental

EIS investigations were performed in a three-compartment electrochemical cell having a saturated calomel electrode (SCE) as a reference electrode and a platinum foil as a counter electrode. The working electrodes were prepared from Zn doped ($p = 1/1.1 \times 10^{19}$ cm^{-3}) and Si doped ($n = 1.2/4 \times 10^{18}$ cm^{-3}) GaAs(100) wafers supplied by AXT Company (GEO Semiconductor (UK) Ltd. and Wafer Technology Ltd. (UK), respectively) mounted on Teflon holders with the rear part and the edges sealed by epoxy resin. Back ohmic contacts to the sample were provided by alloying with Au–Zn alloy (p-doped) and Au–Ge–Ni alloy (n-doped) using the thermal evaporation technique. The GaAs electrodes were previously degreased in acetone, washed with deionized water (Direct-Q 3UV System, Millipore) and etched in a mixture (5 : 1 : 1) $H_2SO_4 : H_2O : H_2O_2$ prior to each experiment. Measurements took place in dark and at room temperature in well deaerated 2 mM hemin in 0.1 M phosphate buffer solution (PBS). The impedance spectra recorded by applying a sinusoid signal with 10 mV amplitude in a frequency interval from 0.3 to 3×10^5 Hz with an IM6 Zahner frequency analyzer have been fitted using the ZView software (Scribner Associates Inc., Southern Pines, N.C.).

XPS investigations were performed with a SPECS spectrometer equipped with a monochromatized Al Kα-anode radiation source operated at 400 W. The wide survey and detail spectra were taken at pressures lower than 2×10^{-9} mbar with pass energy of 100 eV and 10 eV, respectively. The binding energy scale was referenced to the C 1s peak at 285.00 eV. Peaks were resolved with the SDP v7.0 software (XPS International) and assigned by considering reliable literature reports. The spectra were fitted using Voigt peak profiles and either a linear or a Shirley background depending on the background shape.

3. Results and discussion

3.1 Electrochemical investigations

Although the interfacial chemistry at both conduction types of GaAs in various electrolytes is expected to be similar,[18] the profiles of the cyclic voltammograms taken for the p- and n-doped GaAs(100) electrodes in hemin containing PBS solutions show a striking difference. As one may see in Fig. 1, hemin gives rise to a reversible redox process at p-GaAs(100) electrode whereas at the n-doped one, there is only one reduction wave of a considerable lower current density appearing at potential shifted by about 300 mV to more negative values.

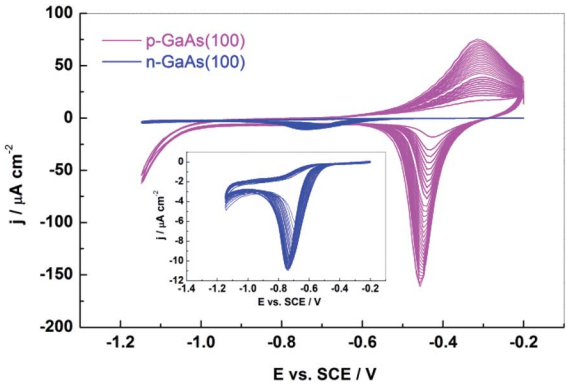

Fig. 1 Cyclic voltammograms of p-GaAs(100) (magenta line) and n-GaAs(100) (blue line) taken at 50 mV s^{-1} in 2 mM hemin in 0.1 M PBS.

The formal potential of −0.36 ± 0.02 V estimated by $(E_{pc} + E_{pa})/2$ for p-GaAs(100) is similar to that obtained with glassy carbon[19] and pyrolitic graphite[20–22] suggesting that chemical nature of the electrode surface does not really influence the formal redox potential of hemin. The differences observed at p- and n-GaAs(100) electrodes may arise from orientation and/or aggregation of hemin molecules adsorbed on the semiconductor surface that could affect the electron transfer rate.[3,4] Hemin may exist in aqueous solution in monomeric or dimeric form causing different adsorption states and thereby different redox potentials in the CV curve.[23–26]

The successive increases in the oxidative and the reductive peak currents at p-GaAs(100) observed during repeated cycling point to the growth of a conductive film on the electrode surface. The surface coverage increases steadily through approximately 30 scans after which the further growth is limited. The films adhere strongly to the electrode surface[11] and are stable to rinsing with aqueous solvents. Similar effects found for the hemin redox process at glassy-carbon or optically transparent SnO_2 electrodes[27] were assigned to a radical cationic polymerization of the peripheral vinyl groups resulting in formation of the polymeric film.[28] Dong and Jiang[29] pointed out that the two vinyls linked to the porphyrin ring may be easily oxidized to radical cationic vinyls on the electrode resulting in a macrocyclic conjugated system since the radical cationic vinyls are conjugated with the porphyrin ring. By collision with another porphyrin molecule it may easily initiate a radical cationic vinyl polymerization. Having a good electroconductivity due to the porphyrin macrocycle conjugation, the polymerized iron porphirin film may facilitate the electron transfer *via* the Fe(III)/Fe(II) couple coordinated to the porphyrin ring on its axes.

Another type of film develops, however, during the repeated scans at n-GaAs(100) electrode. The peak potential shift to more negative values and the rather limited increase of the peak intensity suggest a more resistive constitution and/or another mechanism of formation. Other distinct properties of the films formed at the two types of electrodes were revealed by the EIS investigations on these hemin-modified electrodes. The effect of the applied potential on the phase angle measured at p- and

Open Access Article. Published on 26 March 2020. Downloaded on 2/4/2026 3:08:19 AM.
This article is licensed under a Creative Commons Attribution-NonCommercial 3.0 Unported Licence.

n-GaAs(100) electrodes in hemin solution after the formation of a stable film illustrated in Fig. 2 reveals a clear distinction between them. The phase angle is a highly sensitive indicator of the ionic insulating properties of the organic overlayer.[30–32] At n-GaAs(100), the potential induced changes in the phase angle appear only in the frequency range ($0.3–10^2$ Hz) where the contributions of the dielectric properties of the organic overlayer are expected to prevail.[33,34] The low values of the phase angle in this frequency window over the entire potential range attest the preponderant resistive contributions of the hemin layer formed at n-GaAs(100) electrode to the interfacial impedance in good agreement with the cyclic voltammetry data.

At p-GaAs(100), the phase angle undergoes changes only within a rather narrow potential range close to the current peak observed in the cyclic voltammograms but in the entire frequency range. Such a pronounced dip in the angle phase–frequency plot accompanying the interfacial charge transfer points to major changes not only in the insulating properties of the overlayer but also in the electronic properties of the semiconducting electrode caused by the hemin redox process.

Electron transfer processes at semiconductor electrodes in contact with a redox couple in dark usually occur *via* one of the energy bands depending on the position of the formal potential of the latter one provided that levels of equal energy exist on both sides of the interface.[35,36] The band edges of the clean p-GaAs(100) and n-GaAs(100) in PBS solution (pH 7.5) are situated approximately at the same energy levels since the flat band potential, E_{FB}, of the p-doped one is -0.04 ± 0.02 V and that of the n-doped one is -1.43 ± 0.03 V, the difference between them being equal with the semiconductor bandgap. The formal potential of the redox couple of hemin of -0.36 ± 0.02 V is closer to the valence band edge but, according to Kelly and Notten[37] and Schroeder and Memming,[38] its position cannot provide an optimal overlap with the empty states of this couple since LUMO level of hemin is estimated at ~4.68 eV, *i.e.* ~−0.06 V *vs.* SCE.[39] Surface states localized within the semiconductor bandgap, originating either in defects or adsorbed species, may be, however, as well involved in the charge exchange being able to mediate electron transfer.[36,40–43] Electron transfer occurs, in this case, through population of such levels by either the conduction band in n-type or valence band in p-type semiconductor, yielding different currents for n- and p-GaAs since the concentrations of electrons and holes are dopant dependent.[44] The higher currents found at p-GaAs(100) than at n-GaAs(100) (Fig. 1) might be thus related with the higher dopant concentration of Zn doped GaAs(100) wafers ($p = 1/1.1 \times 10^{19}$ cm^{-3}) than that of the Si doped ($n = 1.2/4 \times 10^{18}$ cm^{-3}) ones, suggesting that the charge transfer involves the valence band in the first case and the conduction band in the latter one.

The presence of the surface states in the GaAs bandgap is notorious. Our previous investigations revealed an important group of donor-like surface states centred at about 0.4 eV above the semiconductor valence band edge,[15,17] at p-GaAs(100) and of another one of acceptor-like surface states located at about 0.7 eV below the conduction band edge at n-GaAs(100).[15,17,45] Quite similar to the deep surface states reported in literature,[46–50] they were associated with a missing Ga defect, As_{Ga}-antisite, considered responsible for the Fermi level pinning on p-GaAs(100),[47] and with an As deficit, Ga_{As}, regarded as the main electron trap in n-GaAs(100),[51] respectively. The difference in their energetic position of 0.3 eV is similar to the difference of about 0.3 V between the potential values at which occurs the cathodic reduction of hemin at the p- and n-GaAs(100) electrodes as seen in Fig. 1. We have analysed the impedance data with the equivalent circuit in Fig. 3, proposed for such a charge transfer process through surface states by Hens[36] and successfully applied by Hens and Gomez[42] at Fe^{3+}/Fe^{2+} reaction at n-GaAs electrode with the only difference that the Warburg impedance is replaced by a constant phase element with CPE-p taken constant (0.5).

As seen in Fig. 4, Mott–Schottky plot is significantly shifted to more negative potentials at the hemin-covered p-GaAs(100)

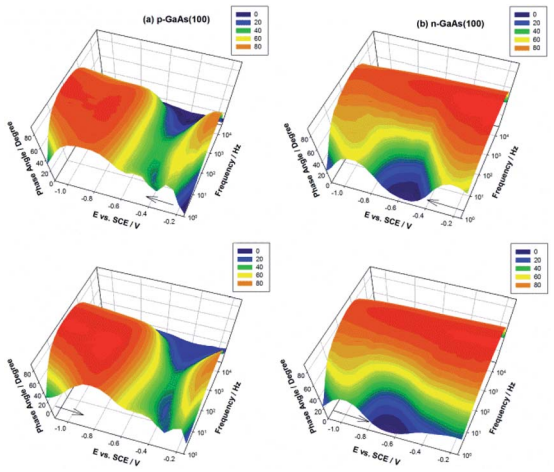

Fig. 2 Effect of the applied potential on the phase angle measured for hemin-covered p-GaAs(100) (left side) and n-GaAs(100) (right side) in 2 mM hemin in 0.1 M PBS during the cathodic (top) and anodic (bottom) scan.

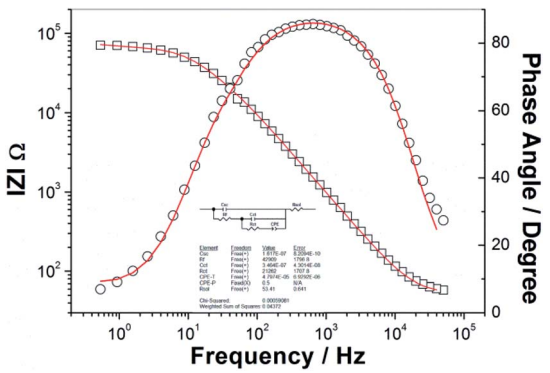

Fig. 3 The equivalent circuit used to model the EIS spectra and a typical example of the fitting parameters, where C_{SC} is the semiconductor space charge capacitance and the subcircuit consisting of R_f, C_{ct}, R_{ct}, and CPE describes the charge transfer,[42] solid lines correspond to the nonlinear least-squares fit and symbols represent the experimental data (□ for |Z| and ○ for phase angle) for n-GaAs(100) electrode in hemin solution at −0.6 V.

This journal is © The Royal Society of Chemistry 2020

Open Access Article. Published on 26 March 2020. Downloaded on 2/4/2026 3:08:19 AM.
This article is licensed under a Creative Commons Attribution-NonCommercial 3.0 Unported Licence.

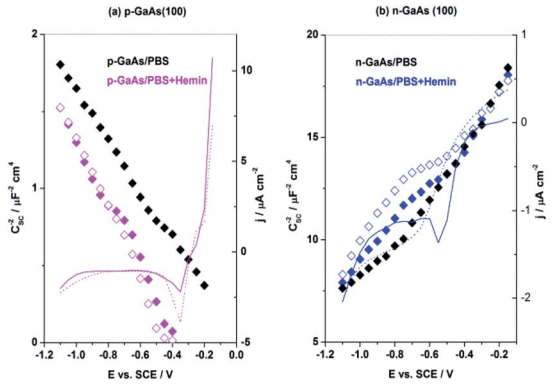

Fig. 4 Mott–Schottky plots and *j*/*E* profiles recorded during the EIS measurements for p-GaAs(100) and n-GaAs(100) in 2 mM hemin in 0.1 M PBS during the cathodic (filled symbols) and anodic (open symbols) potential scans.

electrode but it remains unchanged at the n-doped one before the onset of the potential-induced charge transfer. In principle, the influence of a redox couple on the apparent flat band potential, E_{FB}, could be due either to adsorption of the redox components[52] or to Fermi level pining at the redox potential of the solution couple.[53–57] The shift of E_{FB} up to the redox potential of the hemin/hem couple found at the p-doped hemin-modified electrodes is considered to be the result of the electronic equilibrium between the redox potential of the couple and the semiconductor surface states situated above the valence band edge. In the *j*/*E* profiles recorded during the EIS measurements illustrated in Fig. 4a, one may see that when the bias is applied at the p-doped electrode, the current increases proportionally to the bias, with no threshold. The origin of this highly conductive feature should be indeed the large conductance at the redox process equilibrium and the strong coupling between the electronic states of the adsorbed species with the electrode wave functions. A reversible reaction can only occur if both forward and back reactions *via* one energy band are fast which may happen just for redox systems with the standard potential sufficiently close to one of the energy bands.[58] The observed reversible reaction at hemin covered p-GaAs(100) is explained thus for hemin/hem redox couple by the pining of the semiconductor Fermi level at its standard potential.

The band edge position on the potential scale is clearly a critical parameter for the hemin reduction at GaAs electrodes. A schematic energy diagram is shown in the ESI† in order to provide a suggestive description of the relative position of the conduction (CB) and the valence (VB) band-edges on the electrochemical scale for the bare and the hemin-covered n- and p-GaAs(100) with respect to the formal potential, E^0, of the hemin redox process in PBS solution. The negative shift of the flat band potential caused by the electronic equilibrium between the redox potential of the hem/hemin couple and the semiconductor surface states located above the valence band edge at p-GaAs(100) allows an optimal overlapping of the molecular orbitals of the organic molecule and the valence band of p-GaAs(100) which facilitates the electron capture from the semiconductor valence band within a limited potential range.

At n-GaAs(100) electrode, the band edges remain unchanged before the onset of the charge transfer process. As seen in Fig. 4b, the steep increase of the cathodic current starts around the formal reduction potential of hemin and it is accompanied by a progressive shift to the left of the Mott–Schottky plot. Since the position of the band edges is shifted in the cathodic direction, the matching of energy levels of the redox system with the electronic states of the valence band is expected to be improved suggesting that hemin reduction might proceed in this case directly *via* the valence band electrons. However, the direct hole injection is an unlikely charge-transfer mechanism, at least in this potential range, since it would involve an anodic shift of the flatband potential, as Notten[59] reported for $Fe(CN)_6^{3+}$ reduction at n-GaAs due to accumulation of positive charge at the semiconductor surface. Therefore, the shift to more negative potentials of the Mott–Schottky plot accompanying the pronounced increase of the cathodic current is rather a result of the charge transfer from the conduction band through surface state as Hens and Gomez[42] found as being the most plausible reaction mechanism for the cathodic shift observed at n-GaAs electrodes during the electrochemical reduction of Fe^{3+} to Fe^{2+} ions.

The shifts of E_{FB} upon generation of the reduced species of the redox couple are consistent with Fermi level pinning[53] brought about by surface states localized within the bandgap, and closely related to the changes in the Helmholtz double layer.[60] Vanmaekelbergh[41] demonstrated that for such surface state mediated transfers, it is not possible to separate the electrical impedance in discrete components, due to the strong coupling between the relaxation of the surface state occupancy and the potential drop over the Helmholtz layer. However, the further shift of the Mott–Schottky plot to more negative potential observed at p-GaAs(100) as well the hysteresis found during the anodic potential scan at n-GaAs(100) below −0.6 V suggests changes in the electrical contribution of the Helmholtz double layer to the interfacial impedance, coming from changes in its chemical composition. The potential drop brought about by applied potential at a semiconductor/electrolyte interface is shared by both the semiconductor space charge layer formed beneath the electrode surface and the Helmholtz double layer developed over the electrode surface. As long as the latter one is independent of the applied potential, because either it is much lower than that in the depletion region or its interaction with the semiconducting electrode is weak, changes in the applied potential across the semiconductor solution/interface are primarily reflected in the potential drop across the space charge layer within the semiconductor. However, when the current flow results in significant changes in the Helmholtz double layer composition,[61] these may yield shifts of the energy bands at the semiconductor/electrolyte interface reflected by the flat band potential position. The XPS investigations on the chemical composition of the hemin covered GaAs electrodes brought valuable information in this respect.

Open Access Article. Published on 26 March 2020. Downloaded on 2/4/2026 3:08:19 AM.
This article is licensed under a Creative Commons Attribution-NonCommercial 3.0 Unported Licence.

3.2 XPS investigations

XPS investigations carried on the GaAs substrates after their contact with hemin dissolved in PBS, subsequently rinsed with water and dried in air, revealed significant differences in the chemical bonding of this organic compound with the semiconductor surface driven by the dopant type. The presence of the iron–protoporphyrin adsorbed species on both substrates is certified by the Fe 2p core level region shown in Fig. 5a. The peak of lower binding energy (BE = 711 ± 0.2 eV) is assigned to the Fe(III) $2p_{3/2}$ spin component while that at higher binding energy (BE = 724 ± 0.2 eV) is assigned to Fe(III) $2p_{1/2}$ according to the previous literature reports.[62,63] High broad peak widths at half height are generally characteristics of paramagnetic transition-metal ions due to both the multiplet splitting and the shake-up and the shake-off processes.[64,65] The similar intensity of the Fe 2p core level lines observed on both substrates suggests comparable amounts of adsorbed hemin. Useful information concerning the amount of adsorbed hemin is also provided by the N 1s core-level line (Fig. 5b) coming exclusively from the porphyrin ring. Although the N 1s spectral region is superposed to an Auger structure (Ga $L_2M_{45}M_{45}$) when excited by Al X-ray,[8] the N 1s signal evidences quite well the presence of the hemin species on the sample surface as the signal-to-noise ratio of the 4 nitrogen atoms in the hemin molecule is significant. One may see that besides the species with BE = 398.5 ± 0.2 eV, typical for the nitrogen atom in hemin resident on GaAs substrates,[39] there is another one, with a lower binding energy originating in Ga-Auger emission. The intensity of the Ga-Auger signal in the N 1s spectral region (Fig. 5b) as well as that of the main substrate core-level lines, As 3d and Ga 3d (Fig. 5c), are much lower at p-GaAs(100) than at n-GaAs(100) pointing to a thicker overlayer that may come only from a different adsorption geometry. Taking into account the large difference between the molecular dimensions of hemin, with a height of 1.7 nm and a thickness of 0.3 nm (ref. 66) it is reasonable to suppose a vertical position of the adsorbed molecule on p-GaAs(100) and a planar one on n-GaAs(100).

This conclusion is further supported by comparing the profiles of the As 2p and Ga 2p core level lines taken for hemin adsorbed on p- and n-GaAs(100) substrates illustrated in Fig. 6.

In order to distinguish better the contributions of the hemin bonding, the profiles of the same core-level regions taken for the two substrates after their simple contact with PBS are also shown. The lower kinetic energy of the 2p-lines considerably increases their surface sensitivity as compared to the 3d-lines. One may see that hemin adsorbed on p-GaAs(100) completely suppressed both the substrate core-level lines Ga–As (BE = 1117.3 ± 0.1 eV)/As–Ga (BE = 1323.4 ± 0.1 eV)[67–70] and those of Ga–O (BE = 1118.5 ± 0.1 eV) and As–O (BE = 1326.1 ± 0.2 eV) species,[67–70] which were replaced by two new species with higher binding energies, BE = 1327.1 ± 0.1 eV and BE = 1119.2 ± 0.1 eV, assigned to the carboxylate species As–COO and Ga–COO,[12] respectively. These data suggest that hemin is bound on p-GaAs(100) by its carboxyl groups, known to be responsible for the self-assembled iron porphyrins on the GaAs surfaces.[7,71,72]

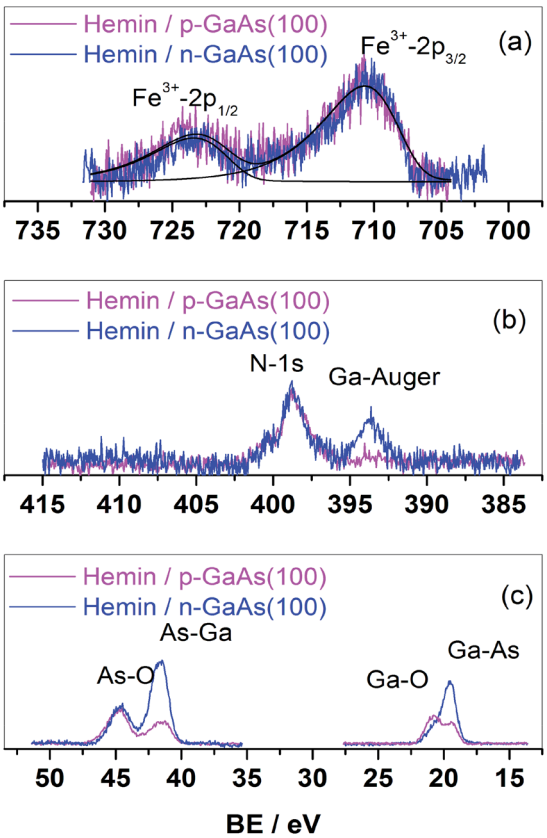

Fig. 5 Fe 2p (a), N 1s (b), Ga 3d and As 3d (c) core level regions for hemin adsorbed on p-GaAs(100) (magenta lines) and n-GaAs(100) (blue lines).

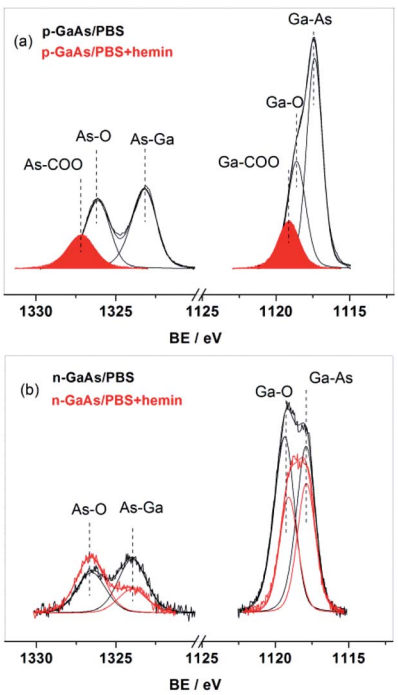

Fig. 6 As 2p and Ga 2p core-level regions for hemin adsorbed on p-GaAs(100) (a) and n-GaAs(100) (b) (red lines); black lines represent the same profiles taken after the contact with PBS.

This journal is © The Royal Society of Chemistry 2020

Open Access Article. Published on 26 March 2020. Downloaded on 2/4/2026 3:08:19 AM.
This article is licensed under a Creative Commons Attribution-NonCommercial 3.0 Unported Licence.

Such species do not appear, however, in the correspondent spectral region on n-GaAs(100), where the adsorbed hemin causes only a decrease in intensity of the substrate core-level lines, As–Ga/Ga–As and a change in their ratio to the oxidation species, As–O and Ga–O, which points to a planar configuration involving only the OH groups of the organic molecule.

The examination of the Fe 2p spectral region of the two GaAs(100) electrodes removed from hemin solution at the two limits of the potential window brings more information concerning their particular interaction with the redox couple. As seen in Fig. 7, each of the two Fe 2p core-level lines is split in two components on p-GaAs(100) electrode. Fe^{2+} and Fe^{3+} species coexist at both limits of the potential window, the reduced one with a relatively higher weigh after the cathodic potential excursion, the oxidized one having a relatively higher weigh after the anodic potential scan. At n-GaAs(100) electrode, however, there is a balance between the two iron species only after the cathodic excursion, whereas after the anodic one, Fe^{3+} species are clearly prevailing.

Surprising is the presence of Cl^- ions on n-GaAs(100) electrode, more pronounced at the negative end of the potential window, as seen in Fig. 8b, unlike the p-GaAs(100) electrode surface where they do not survive the rinsing with water following emersion from the electrolyte solution, no matter the value of the potential is. The Cl 2p spectra recorded in air or after the cathodic and anodic bias is split into $2p_{3/2}$ (BE = 198.1 ± 0.1 eV) and $2p_{1/2}$ (BE = 199.7 ± 0.1 eV) components with 1.6 eV separation[73] representing Cl^- ions.[74]

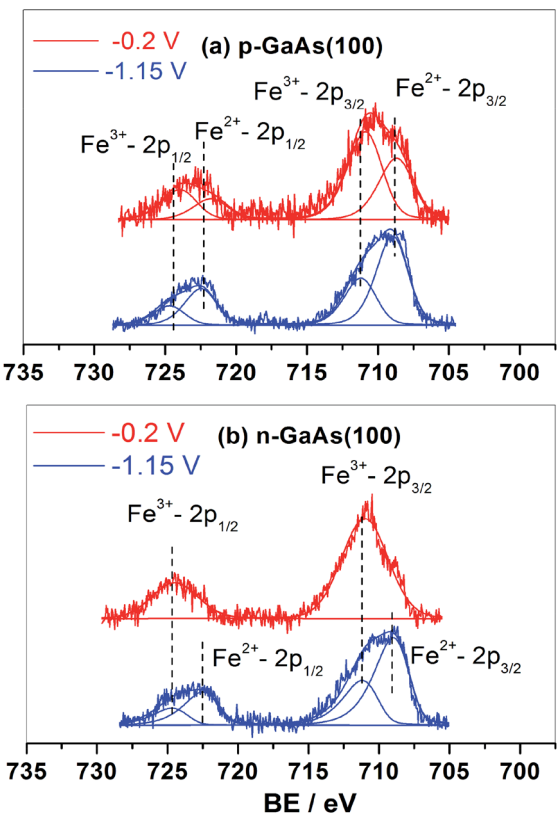

Fig. 7 Fe 2p core-level region for hemin adsorbed on p-GaAs(100) (a) and n-GaAs(100) (b) at the end of the cathodic potential scan (−1.15 V) (blue lines) and at the end of the anodic potential scan (−0.2 V) (red lines).

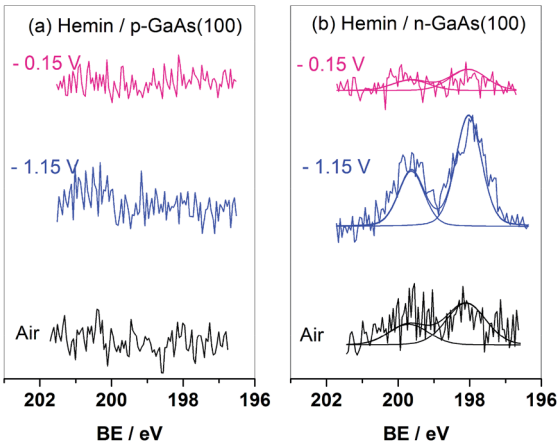

Fig. 8 Cl 2p core-level region for hemin adsorbed on p-GaAs(100) (a) and n-GaAs(100) (b) in air (black lines) and at the end of the cathodic potential scan (−1.15 V) (blue lines) and at the end of the anodic potential scan (−0.2 V) (magenta lines).

The presence of Cl^- ions strengthens the conclusion that Fe^{2+}/Fe^{3+} ions adsorbed at n-GaAs(100) have a quite different adsorption configuration than on p-GaAs(100). The stronger power to attract Cl^- ions suggests a lower spin configuration, that might be favoured by the flat orientation of the adsorbed hemin revealed by lower attenuation of the main substrate core-level lines, As 3d and Ga 3d (Fig. 5c) discussed above. Fe^{3+} ion, which is a d^5 system, may exist in one of four possible spin states: high spin ($S = 5/2$), intermediate spin ($S = 3/2$), low spin ($S = 1/2$) or spin mixed-state,[75,76] depending largely on the axial ligand. Most of the 5-coordinate ferric porphyrins are known to form high-spin complexes with chlorine anion as axial ligand, having the iron atom shifted out of the porphyrin plane toward the ligand.[76,77] The low spin configurations where the ferric atom is located closer to the porphyrin plane provide, however, better overlap with the metal orbitals resulting in an increased bond order and shorter iron–ligand bond lengths, and hence, a high stability.[76] Low-spin ions are expected to bind ligands stronger than high-spin ions not only because they afford better orbital overlap with the pyrrole rings[78] but for there are fewer antibonding e_g electrons too.[79]

4. Conclusions

CV and EIS investigations on the interaction of hemin with GaAs(100) in PBS solution revealed significant differences between p- and n-doped electrodes. Hemin gives rise to a reversible redox process at p-GaAs(100) electrode whereas at the n-doped one, there is only one reduction wave of considerable lower current density appearing at potential shifted to more negative values. The effect of the applied potential on the phase angle pointed out major changes at p-GaAs(100) not only in the insulating properties of the adsorbed layer, as found at n-GaAs(100), but also in the electronic properties of the

Open Access Article. Published on 26 March 2020. Downloaded on 2/4/2026 3:08:19 AM.
This article is licensed under a Creative Commons Attribution-NonCommercial 3.0 Unported Licence.

semiconductor caused by the hemin redox process. Analysis of the experimental data points to a mechanism of charge transfer through surface states,[36] the observed differences being related to the location of the surface states with respect to the formal potential of the hemin redox couple.

XPS data proved that hemin is bound on p-GaAs(100) by its carboxyl groups and adopts a vertical position favourable to a polymeric film formation whereas on n-GaAs(100), the adsorbed hemin has a planar configuration involving mainly the OH groups of the organic molecule which may promote a lower spin state configuration of the Fe ions. Such differences in molecular orientation and spin state configuration are expected to control the coordinating properties of the iron ion and yield significant differences in its catalytic/electrocatalytic reactivity so closely related to the steric and electronic effects of the axial ligands. Therefore, further investigations on the catalytic/electrocatalytic activity of the hemin-functionalized n- and p-GaAs(100) toward NO binding,[7–9] reduction of H_2O_2,[1] hydroxylamine[6] or nitrosamines[5] might open new routes for sensor design approach.

Conflicts of interest

There are no conflicts to declare.

References

1 Z. Brusova and E. Magner, *Bioelectrochemistry*, 2009, **76**, 63–69.
2 G. L. Turdean, I. C. Popescu, A. Curulli and G. Palleschi, *Electrochim. Acta*, 2006, **51**, 6435–6441.
3 J. Chen, U. Wollenberger, F. Lisdat, B. Ge and F. W. Scheller, *Sens. Actuators, B*, 2000, **70**, 115–120.
4 J.-S. Ye, Y. Wen, W. D. Zhang, H.-F. Cui, L. M. Gan, G. Q. Xu and F.-S. Sheu, *J. Electroanal. Chem.*, 2004, **562**, 241–246.
5 X. Su, L. Bromberg, K.-J. Tan, T. F. Jamison, L. P. Padhye and T. A. Hatton, *Environ. Sci. Technol. Lett.*, 2017, **4**, 161–167.
6 B. Kannan, D. Kumsa, A. J. Jebaraj, A. Méndez-Albores, N. S. Georgescu and D. Scherson, *J. Electroanal. Chem.*, 2017, **793**, 250–256.
7 D. G. Wu, D. Cahen, P. Graf, R. Naaman, A. Nitzan and D. Shvarts, *Chem.–Eur. J.*, 2001, **7**, 1743–1749.
8 M. R. Vilar, J. El-Beghdadi, F. Debontridder, R. Naaman, A. Arbel, A. M. Ferraria and A. M. Botelho Do Rego, *Mater. Sci. Eng., C*, 2006, **26**, 253–259.
9 C. Di Franco, A. Elia, V. Spagnolo, G. Scamarcio, P. M. Lugarà, E. Ieva, N. Cioffi, L. Torsi, G. Bruno, M. Losurdo, M. A. Garcia, S. D. Wolter, A. Brown and M. Ricco, *Sensors*, 2009, **9**, 3337–3356.
10 R. Naaman, *Phys. Chem. Chem. Phys.*, 2011, **13**, 13153–13161.
11 A. M. Toader, E. Volanschi, M. F. Lazarescu and V. Lazarescu, *Electrochim. Acta*, 2010, **56**, 863–866.
12 L. Preda, C. Negrila, M. F. Lazarescu, M. Anastasescu, G. Dobrescu, E. Santos and V. Lazarescu, *Phys. Chem. Chem. Phys.*, 2011, **13**, 17104–17114.
13 V. Lazarescu, R. Scurtu, M. F. Lazarescu, E. Santos, H. Jones and W. Schmickler, *Electrochim. Acta*, 2005, **50**, 4830–4836.
14 R. Scurtu, N. I. Ionescu, M. Lazarescu and V. Lazarescu, *Phys. Chem. Chem. Phys.*, 2009, **11**, 1765–1770.
15 V. Lazarescu, A. M. Toader, M. Enache, L. Preda, M. Anastasescu, G. Dobrescu, C. Negrila and M. F. Lazarescu, *Electrochim. Acta*, 2015, **176**, 112–124.
16 V. Lazarescu, M. Enache, M. Anastasescu, G. Dobrescu, C. Negrila and M. F. Lazarescu, *Electrochim. Acta*, 2017, **225**, 551–558.
17 M. Enache, C. Negrila, M. Anastasescu, G. Dobrescu, M. F. Lazarescu and V. Lazarescu, *J. Electrochem. Soc.*, 2018, **165**, H3008–H3017.
18 S. Menezes and B. Miller, *J. Electrochem. Soc.*, 1983, **130**, 517–523.
19 Z. Q. Feng, T. Sagara and K. Niki, *Anal. Chem.*, 1995, **67**, 3564–3570.
20 P. Bianco, J. Haladjian and K. Draoui, *J. Electroanal. Chem.*, 1990, **279**, 305–314.
21 T. Sagara, S. Takagi and K. Niki, *J. Electroanal. Chem.*, 1993, **349**, 159–171.
22 T. Sagara, S. Takeuchi, K. Kumazaki and N. Nakashima, *J. Electroanal. Chem.*, 1995, **396**, 525–533.
23 S. Antoniadou, A. D. Jannakoudakis and E. Theodoridou, *Synth. Met.*, 1989, **30**, 295–304.
24 T. M. Bednarski and J. Jordan, *J. Am. Chem. Soc.*, 1967, **89**, 1552–1558.
25 J. Jordan and T. M. Bednarski, *J. Am. Chem. Soc.*, 1964, **86**, 5690–5691.
26 Z.-X. Liang, H.-Y. Song and S.-J. Liao, *J. Phys. Chem. C*, 2011, **115**, 2604–2610.
27 J. N. Younathan, K. S. Wood and T. J. Meyer, *Inorg. Chem.*, 1992, **31**, 3280–3285.
28 K. A. Macor and T. G. Spiro, *J. Am. Chem. Soc.*, 1983, **105**, 5601–5607.
29 S. Dong and R. Jiang, *J. Inorg. Biochem.*, 1987, **30**, 189–201.
30 E. Boubour and R. B. Lennox, *Langmuir*, 2000, **16**, 4222–4228.
31 E. Boubour and R. B. Lennox, *Langmuir*, 2000, **16**, 7464–7470.
32 I. Burgess, B. Seivewright and R. B. Lennox, *Langmuir*, 2006, **22**, 4420–4428.
33 E. Boubour and R. B. Lennox, *J. Phys. Chem. B*, 2000, **104**, 9004–9010.
34 M. Luo, A. Amegashie, A. Chua, G. K. Olivier and J. Frechette, *J. Phys. Chem. C*, 2012, **116**, 13964–13971.
35 R. Memming, *Electrochim. Acta*, 1980, **25**, 77–88.
36 Z. Hens, *J. Phys. Chem. B*, 1999, **103**, 122–129.
37 J. J. Kelly and P. H. L. Notten, *Electrochim. Acta*, 1984, **29**, 589–596.
38 K. Schroeder and R. Memming, *Berichte der Bunsengesellschaft für physikalische Chemie*, 1985, **89**, 385–392.
39 M. A. Garcia, M. Losurdo, S. D. Wolter, T. H. Kim, W. V. Lampert, J. Bonaventura, G. Bruno, M. Giangregorio and A. Brown, *J. Vac. Sci. Technol., B: Microelectron. Nanometer Struct.–Process., Meas., Phenom.*, 2007, **25**, 1504–1510.
40 D. Vanmaekelbergh, *Electrochim. Acta*, 1997, **42**, 1121–1134.
41 D. Vanmaekelbergh, *Electrochim. Acta*, 1997, **42**, 1135–1141.

 This journal is © The Royal Society of Chemistry 2020

Open Access Article. Published on 26 March 2020. Downloaded on 2/4/2026 3:08:19 AM.
This article is licensed under a Creative Commons Attribution-NonCommercial 3.0 Unported Licence.

42 Z. Hens and W. P. Gomes, *J. Phys. Chem. B*, 1999, **103**, 130–138.
43 A. J. Bard, F.-R. F. Fan, A. S. Gioda, G. Nagasubramanianand and H. S. White, *Faraday Discuss. Chem. Soc.*, 1980, **70**, 19–31.
44 P. A. Kohl and A. J. Bard, *J. Electrochem. Soc.*, 1979, **126**, 59–67.
45 V. Lazarescu, M. F. Lazarescu, E. Santos and W. Schmickler, *Electrochim. Acta*, 2004, **49**, 4231–4238.
46 S. P. Svensson, J. Kanski, T. G. Andersson and P.-O. Nilsson, *J. Vac. Sci. Technol., B: Microelectron. Process. Phenom.*, 1984, **2**, 235–239.
47 T. M. Valahas, J. S. Sochanski and H. C. Gatos, *Surf. Sci.*, 1971, **26**, 41–53.
48 K. J. Choi and J.-L. Lee, *Appl. Phys. Lett.*, 1999, **74**, 1108–1110.
49 E. R. Weber, H. Ennen, U. Kaufmann, J. Windscheif, J. Schneider and T. Wosinski, *J. Appl. Phys.*, 1982, **53**, 6140–6143.
50 T. E. Kazior, J. J. Lagowski and H. C. Gatos, *J. Appl. Phys.*, 1983, **54**, 2533–2539.
51 J. O. McCaldin, T. C. McGill and C. A. Mead, *Phys. Rev. Lett.*, 1976, **36**, 56–58.
52 R. McIntyre and H. Gerischer, *Berichte der Bunsengesellschaft für physikalische Chemie*, 1984, **88**, 963–969.
53 G. Nagasubramanian, B. L. Wheeler, F.-R. F. Fan and A. J. Bard, *J. Electrochem. Soc.*, 1982, **129**, 1742–1745.
54 A. J. Bard, A. B. Bocarsly, F.-R. F. Fan, E. G. Walton and M. S. Wrighton, *J. Am. Chem. Soc.*, 1980, **102**, 3671–3677.
55 F.-R. F. Fan and A. J. Bard, *J. Am. Chem. Soc.*, 1980, **102**, 3677–3683.
56 B. Ba, B. Fotouhi, N. Gabouze, O. Gorochov and H. Cachet, *J. Electroanal. Chem.*, 1992, **334**, 263–277.
57 G. Nagasubramanian, B. L. Wheeler and A. J. Bard, *J. Electrochem. Soc.*, 1983, **130**, 1680–1688.
58 D. Meissner and R. Memming, *Electrochim. Acta*, 1992, **37**, 799–809.
59 P. H. L. Notten, *Electrochim. Acta*, 1987, **32**, 575–581.
60 H. H. Goossens, W. P. Gomes and F. Cardon, *J. Electroanal. Chem.*, 1990, **278**, 335–349.
61 I. Uhlendorf, R. Reineke-Koch and R. Memming, *J. Phys. Chem.*, 1996, **100**, 4930–4936.
62 M. Aronniemi, J. Sainio and J. Lahtinen, *Surf. Sci.*, 2005, **578**, 108–123.
63 T. Yamashita and P. Hayes, *Appl. Surf. Sci.*, 2008, **254**, 2441–2449.
64 K. M. Kadish, L. A. Bottomley, J. G. Brace and N. Winograd, *J. Am. Chem. Soc.*, 1980, **102**, 4341–4344.
65 T. A. Carlson, *Photoelectron and Auger Spectroscopy*, Plenum Press, New York, 1975.
66 D. L. Compton and J. A. Laszlo, *J. Electroanal. Chem.*, 2002, **520**, 71–78.
67 B. A. Cowans, Z. Dardas, W. N. Delgass, M. S. Carpenter and M. R. Melloch, *Appl. Phys. Lett.*, 1989, **54**, 365–367.
68 J. S. Ha, S.-J. Park, S.-B. Kim and E.-H. Lee, *J. Vac. Sci. Technol., A*, 1995, **13**, 646–651.
69 G. Nesher, A. Vilan, H. Cohen, D. Cahen, F. Amy, C. Chan, J. Hwang and A. Kahn, *J. Phys. Chem. B*, 2006, **110**, 14363–14371.
70 T. Aqua, H. Cohen, O. Sinai, V. Frydman, T. Bendikov, D. Krepel, O. Hod, L. Kronik and R. Naaman, *J. Phys. Chem. C*, 2011, **115**, 24888–24892.
71 R. Cohen, S. Bastide, D. Cahen, J. Libman, A. Shanzer and Y. Rosenwaks, *Adv. Mater.*, 1997, **9**, 746–749.
72 D. G. Wu, G. Ashkenasy, D. Shvarts, R. V. Ussyshkin, R. Naaman, A. Shanzer and D. Cahen, *Angew. Chem.*, 2000, **112**, 4670–4674.
73 G. Beamson and D. Briggs, *High Resolution XPS of Organic Polymers*, John Wiley & Sons Ltd., Chichester, 1992.
74 J. F. Moulder, W. F. Stickle, P. E. Sobol and K. D. Bomben, *Handbook of X-ray photoelectron spectroscopy*, ed. J. Chastain, Perkin-Elmer Corporation, Physical Electronics Division, Minnesota, 1992, p. 62.
75 W. R. Scheidt and M. Gouterman, in *Iron Porphyrins Part 1*,ed. H. Gray and A. B. P. Lever, Elsevier, New York, 1983.
76 J. W. Owens and C. J. O'Connor, *Coord. Chem. Rev.*, 1988, **84**, 1–45.
77 R. F. Pasternack, B. S. Gillies and J. R. Stahlbush, *J. Am. Chem. Soc.*, 1978, **100**, 2613–2619.
78 C. L. Coyle, P. A. Rafson and E. H. Abbott, *Inorg. Chem.*, 1973, **12**, 2007–2010.
79 L. M. Epstein, D. K. Straub and C. Maricondi, *Inorg. Chem.*, 1967, **6**, 1720–1724.